We are IntechOpen, the world's leading publisher of Open Access books Built by scientists, for scientists

4,800
Open access books available

122,000
International authors and editors

135M
Downloads

Our authors are among the

154
Countries delivered to

TOP 1%
most cited scientists

12.2%
Contributors from top 500 universities

WEB OF SCIENCE™

Selection of our books indexed in the Book Citation Index in Web of Science™ Core Collection (BKCI)

Interested in publishing with us?
Contact book.department@intechopen.com

Numbers displayed above are based on latest data collected.
For more information visit www.intechopen.com

3

Interferometric Imaging Technology for Microwave Radiometers

Ji Wu, Hao Liu, Jingye Yan, Cheng Zhang and Weiying Sun
Center for Space Science and Applied Research,Chinese Academy of Scienses
China

1. Introduction

Since 1957, when the first man made satellite opened the space age of human history, satellite earth observation has been taking advantage of high altitude to look at the globe and have applications in the areas of weather forecasting, oceanography, land survey and resource discovery, environmental and disaster monitoring, as well as applications in the area of defence. The observational frequency bands have coverage in microwave, through infrared and visible light, up to ultraviolet.

Among all frequency bands, microwave has special characteristics. Besides its all weather and all time ability, it also has the ability to penetrate the surface canopy and even the ground while the frequency is approaching the low end. It is also capable and easy to realize polarized measurement which increases the ability to identify the internal information of the observed targets. The spatial resolution for synthetic aperture radar has already reached the level in the order of meters or decimetres, comparable to optical sensors.

However, the active microwave sensors, such as synthetic aperture radar, have disadvantage in its high power consumption due to high transmission power and heavy mass which require many resources from spacecraft.

Another kind of microwave sensor is a passive sensor, also called a radiometer. It is basically a very high sensitivity noise receiver. By integrating the received noise from the observed scene over time, the characteristics of different scenes and targets, for example if the water content in clouds or soil changed, will be abstracted by the sensor through the variations of the integrated noise levels. The longer the integration is done, the more sensitivity the sensor would have. According to Planck's Law, all natural objects with temperature should have radio emissions independent of the Sun and any active radio illumination. This radio emission is called the brightness temperature and is related to both the physical temperature and the characteristics of the materials. The brightness temperature in the microwave bands are a very sensitive parameter to water, no matter whether it is in the air or in the soil. If different microwave band is applied, the brightness temperature is also sensitive enough to reflect the surface roughness that has a correlation length around the wavelength. Once the polarization information is acquired, more

information can be abstracted from the emission such as ocean surface wind direction. Since the radiometer is a receiver only, it does not require high power. In fact, a radiometer takes much less power and mass resources from a spacecraft than that of active microwave sensors.

The passive microwave sensor also has disadvantages. Due to its nature as a passive sensor and the incoherent feature of the noise signal from microwave emission of the ground materials, the radiometer cannot apply the principle of synthetic aperture radar (SAR) to reach very high spatial resolution. Its spatial resolution is closely related to the physical size of the receiving antenna, i.e. the half power beam width of the antenna at the working frequency. For instance, if an L band (f_o = 1.4 GHz) radiometer has a receiving antenna of 2 meters in diameter, and working in a low Earth orbit at an altitude of 800km, the spatial resolution on the surface of the ground is no better than 85km. For this reason, in spite of the many advantages of passive microwave remote sensing, microwave radiometers can only be used in the area of ocean, atmosphere and land soil moisture observations where no high spatial resolution is required.

The same difficulty had already been recognized in the area of astronomy where the location of stars with strong radio emission would likely be detected. From the 1950s to the 1960s, a technology called interferometric imaging had been developed (Thompson et al, 1986). The basic principle is to measure the scene indirectly, not in its spatial domain but in its spatial frequency domain, called the u-v plane. After the measurement, a Fourier transform is performed to get the original scene. The quantity which has been measured in the Fourier domain is called the Visibility Function by the astronomers. This name was carried on when this technology was introduced to the area of Earth observation in the 1980's (Ruf et al, 1988).

The measurements, or sampling, in the spatial frequency domain can be carried out with a basic tool of two coherent receiving channels with small element antennas and a complex correlator. The coherent receiving channels mean they use the same local oscillator. The complex correlator carries a multiplication function with the output signals from the two receivers and giving two outputs I and Q representing the real part and the imaginary part of the complex value of the multiplication output. The two small element antennas form a baseline in space. The length of it (the distance between the phase centres of the two antennas) represents the radius of a sampling point in the u-v plane, while the orientation of the baseline represents the polar angle of this sampling point in the u-v plane. With these two values, i.e. the module and polar angle, a sampling point is exclusively defined. In practice, one element can be used more than one time to take many samples while combining with other different elements and forming different baselines. In this way, the antenna array with small antenna elements can be much thinned. As astronomers did, a Y shaped two dimensional linear array can definitely represent a full 2-D array and there is no need to scan the antenna mechanically since field of view of this system is the element antenna pattern which already covers a wide area of interest.

Another attractive quality of the interferometric imaging technology is that the physical aperture of the thinned array of the interferometric imaging system can be reduced by half compared with traditional radiometers. A direct explanation of this is because the beam width of each of the grating-lobes of the interferometer is only 1/2 of a traditional two

element array where the outputs of the two elements are added, not multiplied. Mathematical explanation will be given in the following section.

These are what interested Earth observation sensor engineers. A large thinned array can be folded during launch and redeployed in orbit and no mechanical scan during the observation is needed. Plus the characteristics of having only 1/2 of the traditional physical aperture, the interferometric imaging radiometer can reach a much higher spatial resolution than traditional radiometer technology can do. In order to avoid confusion with the already established phrase 'synthetic aperture' for active microwave radars, this technology is called interferometric imaging technology most of the time. Occasionally it is also called the interferometric synthetic aperture radiometer, or simply synthetic aperture radiometer.

In this chapter, we will start with the basic principles of this technology by talking about the spatial frequency property of an image. This approach is different from other documentation dealing with this topic and easy to understand by the readers with basic knowledge of Fourier transformation. In the third Section, we deal with the basic sampling technologies and its characteristics. In the fourth Section, the sampling technique is integrated into systems. Different sampling systems are introduced with emphases on time shared systems, particularly on the clock scan system which is our original contribution to this technology. In Section five, image reconstruction algorithms are introduced with the emphases on interpolation technology when the samples in the u-v plane are not on a rectangular grid. In Section six, some future applications of this new technology are introduced. All of them are associated with current real mission studies and some of them will certainly become real missions in the future.

2. Basic theorem

If we look down, what we see from space is the Earth. For middle or low resolution earth observation, the images that we get are mainly the scenes of the land or the oceans. In this Chapter, only gray scale image or fake colour image that represent brightness temperature levels are discussed.

The variations of the image's gray scale and texture represent the variations in spatial frequencies. Fast variations (with fine texture) correspond to high spatial frequencies, while gentle variations (with coarse texture) correspond to low spatial frequencies. The directionality of the texture variation represents the two-dimensional property of the spatial frequency. The contrast of the texture represents the intensity of the corresponding spatial frequency. The Fourier transform of a two-dimensional image is its spatial frequency spectrum, as illustrated in Fig. 1, in which the coordinates of the original spatial image are represented by (x-y), while the coordinate of the spatial frequency spectrum are represented by (u-v). The spatial frequency spectrum is also known as spatial frequency domain image, or u-v domain image.

The spatial frequency domain image is centred at the origin, and each point corresponds to a spatial frequency of the original image. For a vector from origin to a point in spatial frequency domain, the length represents the value of the spatial frequency, i.e. the spatial frequency becomes lower when the vector moves toward the origin, which can be defined as

the low frequency component; and conversely, the spatial frequency becomes higher when the vector moves away from the origin, which can be defined as the high frequency component. As illustrated in Fig.2, the angle between the vector and v-axis in the spatial frequency domain corresponds to the angle between the image texture and the x-axis in the spatial domain, while the amplitude at the vector point in the spatial frequency domain represents the amplitude of the corresponded image texture in spatial domain. So, each point in spatial frequency domain contains its own practical physical meaning, and the information it takes covers all over the image in spatial domain, not only to one single point.

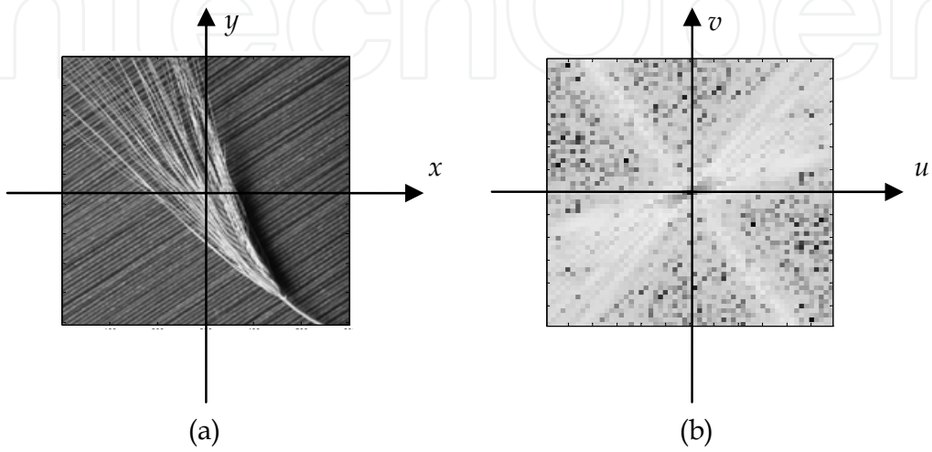

Fig. 1. Original Spatial image (a) and its spatial frequency spectrum image (b)

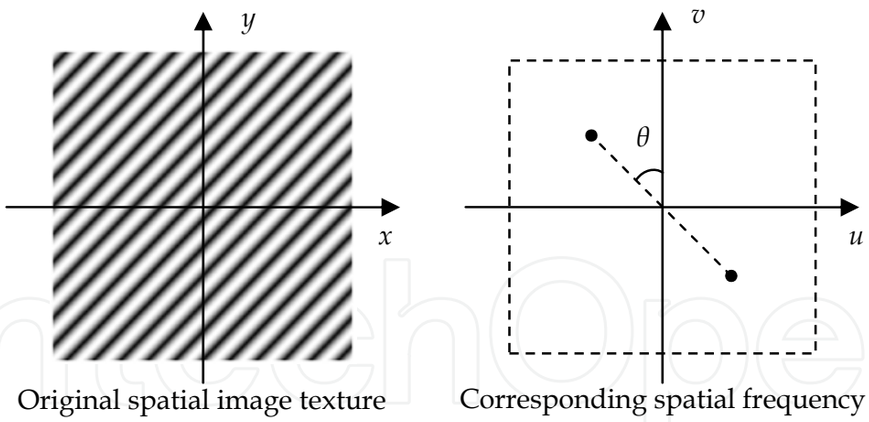

Fig. 2. Image texture and its spatial frequency

The basic principle of the interferometric passive imaging technology is to conduct measurement in spatial frequency domain, and then retrieve the original image in spatial domain by Fourier transform.

As same as the direct measurement on the original image in spatial domain, the spatial resolution of any measurement system is limited. An interferometric passive imaging system can get only limited samples in spatial frequency domain. The maximum u-v value

sampled is the highest spatial frequency which corresponds to the highest spatial resolution of the retrieved image. According to the sampling principle, the least sampling spacing can also be determined.

According on the Fourier transform theory, the spatial frequency spectrum has the following properties:

1. Conjugate symmetry: F(u,v) =F *(-u,-v)
2. Periodicity: F(u,v) =F(u+M,v) =F(u,v+N) =F(u+M,v+N)

The complex conjugate symmetry property implies that, when we conduct sampling in the spatial frequency domain, only half of the frequency spectrum in u-v plane is needed, and another half can be achieved mathematically by conjugate symmetry. In other words, once we sample a point in spatial frequency domain, we simultaneously get another sample at the conjugate symmetric point. By this method, the sampling efficiency can be significantly improved.

The conjugate symmetry property also explains why the interferometric imaging system has only 1/2 of the physical aperture than traditional ones but still get the same spatial resolution. This is because, due to the symmetry, the areas sampling points are doubled in the spatial frequency domain, the u-v plane. Once the Fourier transform is done, one gets the same number of points in the spatial domain, which means the retrieved image also gets double points. Put in simplified terms, this means measure one half, but get one. The size of the physical aperture in the interferometric sampling system is naturally reduced by half.

The periodicity property implies that, periodical extension, or namely aliasing, will appear after the Fourier transform in the retrieved image. Therefore, we must pay attention to the concerned image region, in which aliasing should not be included. In addition to selecting proper sample spacing, element antenna patterns can also be used to weigh the observation field of view, and then restrict the unwanted aliasing image.

3. Sampling measurement in spatial frequency domain

The purpose of sampling measurement in the spatial frequency domain is to get every point on a sampling grid in the spatial frequency domain, except the ones that can be obtained by complex conjugate symmetry. Since a single point in the spatial frequency domain corresponds to a specific image texture, as shown in Fig. 2, it can be measured by a two-element array which has a fringe-shaped beam. This array is also called a two-element interferometer, whose block diagram and fringe-shape pattern are illustrated in Fig. 3.

In the figure, the coherent receiving channels are simplified to two antennas only. The function of the complex correlator is to conduct complex multiplication of the signals received from the two antennas, with their original phases. The pattern of this interferometer is called the fringe function. If the length of the baseline is increased, the number of the grating-lobes of the Fringe Function increases too, and the width of each lobe decreases.

Since different spatial frequencies correspond to different image textures, the interferometers with different baseline lengths can measure the image texture characteristics corresponding to different Fringe Functions. When the baseline's length is increasing, the number of grating-lobes and the spatial frequency are both increasing. In other words, the long baseline interferometer can measure the high frequency component in the spatial frequency domain of the original image, while the short baseline interferometer can measure the low frequency component. So, by utilizing the combination of all the interferometers with different baselines' lengths and directions, the full sampling coverage on the spatial frequency domain of an original image can be achieved.

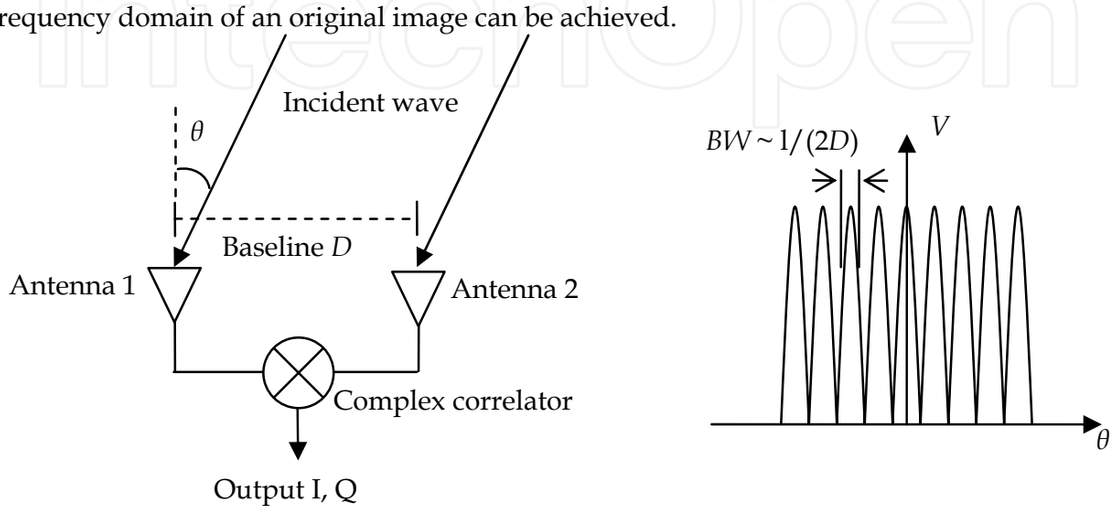

(a) Block diagram of an interferometer (b) Pattern of an interferometer

Fig. 3. Schematic diagram of two-element interferometer (a) and its pattern (b)

It should be mentioned here that the beam width of a lobe of the fringe function is 1/2D, which is half of the traditional two element array. This enables the interferometric imaging radiometer to use only 1/2 of the physical array aperture, i.e. the longest baseline in the system, to get the same spatial resolution that can be reached by the traditional radiometer.

Further theoretical analysis on the interferometric measurement can be applied. The ideal measurement output of a two-element interferometer is expressed as (Corbella et al, 2004),

$$V(u,v)=\iint \frac{T_B(\xi,\eta)}{\sqrt{1-\xi^2-\eta^2}}\exp(-j2\pi(u\xi+v\eta))dudv \qquad (1)$$

in which $V(u, v)$ is the so-called visibility function, $(u, v) = (x_1-x_2, y_1-y_2)/\lambda$ is the baseline vector normalized by the wavelength, $(\xi, \eta)=(\sin\theta\cos\varphi, \sin\theta\sin\varphi)$ is the direction cosine of the incident wave, $T_B(\xi, \eta)$ is the brightness temperature distribution of the scene and the targets. The Fourier relationship between the visibility functions and the brightness temperature distribution is obvious. Each baseline corresponds to two spatial frequency sampling positions in the u-v plane, i.e. (u, v) and $(-u, -v)$. The brightness temperature distribution of the scene and the targets can be retrieved by Fourier transform after a full sampling measurement in the spatial frequency domain.

Only some discrete points in the spatial frequency domain can be sampled by interferometric measurement. According to Fourier transform principle, the maximum sample spacing $u_{\max}$ (longest baseline) determines the spatial resolution of the retrieved image, while the lowest sample spacing Δu (shortest baseline) determines the aliasing-free field of view (AF-FOV), as illustrated in Fig. 4.

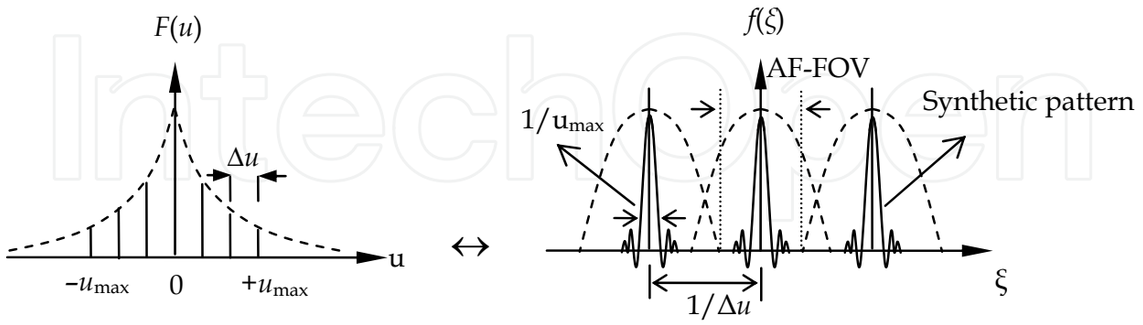

(a) Visibility function samples (b) Periodical extension of the retrieved image

Fig. 4. Visibility function sampling and image aliasing

In order to realize spatial resolution $\Delta\xi$, and also ensure no aliasing in the $2\xi_{max}$ region, the longest and shortest baselines of the interferometric measurement should satisfy the following requirements,

$$u_{\max} > \frac{1}{\Delta\xi}, \qquad \Delta u < \frac{1}{2\xi_{\max}} \tag{2}$$

Limited sampling coverage is equivalent to a sharp cut-off in the spatial frequency domain, which can cause the so-called Gibb's phenomenon. In general, the Gibb's phenomenon can be mitigated by a windowing operation on visibility functions. Some specific window functions can be applied on the measured visibility function samples, which can reduce the side-lobe level of the synthesized pattern, but also broaden the main beam and reduce the spatial resolution of the image. Some commonly used window functions include: Hanning, Hamming, Blackman, Kaiser and some other functions (Harris, 1978 and Anterrieu et al, 2002). Different window functions can achieve a different balance between the side-lobe level and main beam width. Another purpose of introducing window functions is to realize multi-resolution observation with the same observational dataset: to retrieve images with different spatial resolutions according to different application requirements (Ribo, 2003). Taking MIRAS of the SMOS mission as an example, the spatial resolution for land applications and ocean applications are different.

4. Passive interferometric imaging system

Array configuration plays a key role in an interferometric imaging system. One of the major goals of the interferometric imaging radiometer design is to take as much coverage of the u-v plane as possible while at the same time to use as few element antennas as possible. Since the observation target is located in the far field of the antenna array, the correlation output of any pair of antenna elements is equivalent if they compose the same baseline (both

in length and direction) no matter where they are locally placed. This means that the correlation output is independent of the location from which the interferometer takes the visibility samples. To acquire the entire coverage of the harmonics in the spatial frequency domain, only one visibility is necessary for each harmonic. Therefore, the designer of an interferometric imaging radiometer system always tries to reduce the redundant baselines and use as few element antennas as possible. This is also one of the major jobs for the design of the system.

4.1 One dimensional push-broom imaging system

A one dimensional push-broom is a combined design of both traditional radiometers and interferometric imaging radiometers. In other words, the interferometric imaging technology is only applied in the cross track direction, the resolution in the along track direction is still obtained by traditional real aperture technology. Therefore, the element antennas of the array should be a fan beam with a broad beam in the cross track direction and narrow beam in the along track direction. For this kind of beam, the most common design is to have a slotted waveguide as the stick element antenna at the commonly used microwave bands. The waveguides are placed in the along track direction, as see in Fig. 5. In the cross track direction, the waveguides are arranged according to the design principle of interferometric technology which will be discussed below. This kind of imaging system is usually called 1 D push-broom imaging system. In this case, the spatial frequency domain reduced also from 2D to 1D, i.e. the u-v plane became u-axis only.

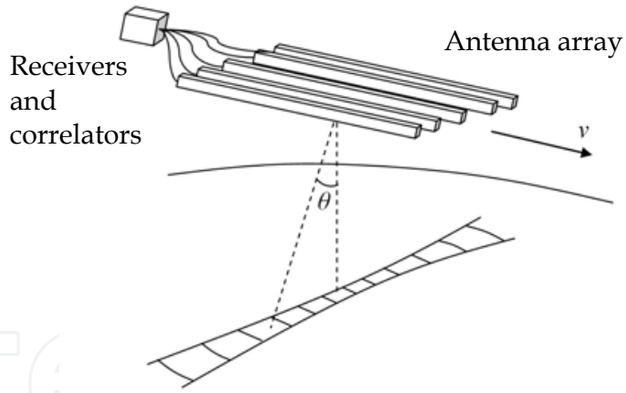

Fig. 5. One dimensional push-broom imaging system

As it is discussed in the previous sections, the ultimate objective of applying interferometric technology is to reduce the number of array elements. It is also known that the sampling of each special frequency component need not be duplicated, although there is always some redundancy in practice. An array configuration design example of a one dimensional push-broom imaging system is shown in Fig. 6. There one can see, with a 5 element antenna placed in a special way, all frequency components from 1 Δu up to 9 Δu are all sampled by taking different combinations of the element antennas. The dashed lines show the missing elements from a full array if a conventional array design was applied. You can also fund that there are redundant baselines, such as between elements 2 and 3, the baseline is also 3

Δu, the same that is shown between elements 3 and 4. However, the redundant baselines cannot be further eliminated, we can take advantage of having them by averaging the outputs given by the redundant baselines. In this way the sensitivity of the system will be increased.

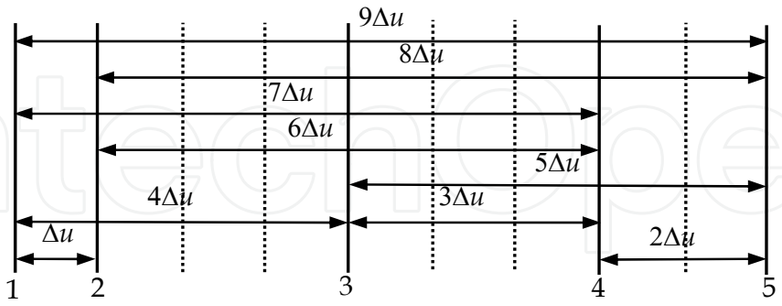

Fig. 6. 5 antenna elements comprise 9 baselines

In general, for a N elements antenna system, if we take the combination of any two of them, there are $N(N-1)/2$ different ways. If those baselines are all independent from each other, i.e. if they cover from $1\ \Delta u$ to $N(N-1)/2\ \Delta u$ in the 1-D case, this system is called a zero redundancy array system. Unfortunately zero redundancy exists only if the number of antenna's elements is less than 4 for 1-D case, as shown in Fig.7.

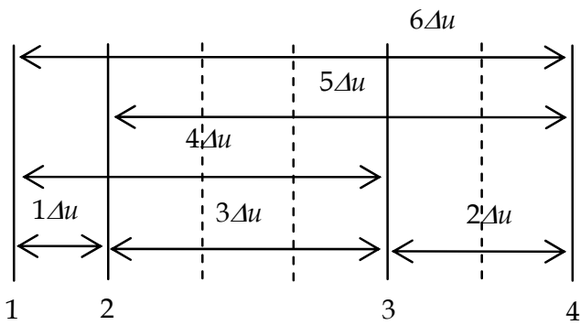

Fig. 7. A zero redundant thinned array with 4 element antennas

When there are more than 4 antenna elements, an optimization process is necessary in order to find the best design that uses as few elements as possible. The optimization process becomes complicated when the spatial resolution gets better thus the size of the array increases. A mathematic algorithm to compute the minimum redundancy array for any size has so far not been found (Ishiguro, 1980). An effective tool to search the minimum redundancy array is with the aid of a computer. Non-linear methods such as the simulated annealing algorithm and genetic algorithm have been developed to optimize the array configuration. Optimum configuration of element antenna positions with an array element $N \leqslant 30$ are given by (Ruf, 1993), which can be applied in different applications.

The first ever 1 D interferometric imaging system for Earth observation is the Electronically Scanned Thinned Array Radiometer - ESTAR. ESTAR was developed as part of the cooperative research between the NASA/Goddard Space Flight Center and the University

of Massachusetts at Amherst (Le Vine, 1994, 2004). ESTAR is an L-band (1.4GHz) instrument. Five antenna elements comprise 7 baselines and result in an equivalent half power beam width (HPBW) of 7°. ESTAR flew on the NASA P-3B Orion aircraft in the 90's to demonstrate the imaging principles. Lots of measurement data were obtained for retrieval of soil moisture (Le Vine et al, 2001; Guha et al, 2003) and ocean salinity (Le Vine et al, 2000a). Results are consistent with values of soil moisture observed in-situ at the observed sites with previous measurements in the same area. ESTAR demonstrated that the passive interferometric technique is feasible. A follow-up project to ESTAR, called HydroSTAR, was proposed by NASA in 1998. It would have been a space borne 1-D interferometric imager for the Earth System Science Pathfinder (ESSP) mission (Le Vine, 1999). HydroSTAR was later cancelled due to technical risk and other none technical reasons.

One dimensional interferometric radiometers at higher frequency bands were built at the Center for Space Science and Applied Research (CSSAR), Chinese Academy of Sciences (CAS). Push-broom type C-band and X-band radiometers were completed in 2001 and 2004, respectively (Dong, 2000; Liu, 2004; Wu, 2005a), as shown in Fig.8. Flight tests were conducted and the brightness temperature images were acquired. The C-band interferometric radiometer works at 6.6GHz. Its 6 antenna elements form 10 baselines (zero baseline was not taken into account). The HPBW of the C-band radiometer is 4°. The X-band imager works at 9.4GHz with 8 antenna elements and 19 baselines resulting in a 2° HPBW.

(a) (b)

Fig. 8. One dimensional interferometric radiometers built by CSSAR

Another X-band interferometric radiometer, the X-Band Lightweight Rainfall Radiometer (LRR-X) is an airborne microwave sensor that is developed for the NASA Earth Science Technology Office by Goddard Space Flight Center and the University of Michigan (Ruf & Principe, 2002, 2003). LRR-X is intended to address several pressing issues related to the Global Precipitation Measurement (GPM) Mission. It is a science and technology testbed instrument. LRR-X is also a push-broom imager operating at 10.7 GHz with a ± 45 cross track field of view and a nominal 1.5° angular resolution at its nadir.

4.2 Two dimensional snapshot interferometric radiometer

One dimensional interferometric radiometer uses thinned array only in the cross track direction. Thus the dimension in along track direction is still large, as it can be seen from Fig.8. In order to further reduce the physical size of the antenna, two-dimensional interferometric radiometer has been developed. As it is discussed in sections 2 and 3, 2-D interferometric radiometer takes measurement in the full u-v plane. Therefore, it will have thinned antenna array and 1/2 apertures in both directions. If the sampling baseline can cover all angles and lengths within the upper limit that can be provided by the physical aperture, the image will be taken like a camera, or called snapshot imaging.

To provide full coverage with samplings distributed in grid in the spatial frequency domain, many array configurations are employable, such as T-shape, U-shape, Y-shape, Δ-shape and so on. Among those, T and U shaped arrays produce visibility function samples in a rectangular grid in the u-v plane, while the Y and Δ-shape arrays produce the visibility function samples in a triangular grid. Classical fast Fourier transform in rectangular grid is applicable for retrieving the brightness temperature image in the spatial domain. Hexagonal fast Fourier transform is also applicable in a triangular grid. Y-shape array has been adopted by many systems due to the unique advantage that the array thin factor is the best among all the 2-D configurations. However, none of those configurations can reach zero redundancy. Redundant baselines, particularly at the lower spatial frequency components, are used to average the noise, which is equivalent to an increase in the integration time.

2D-STAR was developed under NASA's Instrument Incubator Program (IIP) at the Goddard Space Flight Center. As the next generation instrument of ESTAR, 2D-STAR is an experimental instrument for evaluating techniques and applications of 2D aperture synthesis (Le Vine et al, 2000b, 2004). 2D-STAR works at L-band with two polarizations and does aperture synthesis in both directions (cross track and along track). Micro-strip patch antenna is selected as the element antenna, and the minimum element spacing Δu is 0.5λ. A square shaped full array of 11×11 elements provide the flexibility to compare between different array configurations, including Y, T, U, etc. The instrument made its maiden flight in 2002 and participated in a series of field tests in 2003 and 2004 flying over research sites in Alabama, Georgia and Oklahoma during SMEX-03 and SMEX-04 campaigns, respectively (Le Vine et al, 2007).

HUT-2D was developed by the Helsinki University of Technology (HUT), Finland (Rautiainen et al, 1999, 2003). Development began in the late 1990s and was completed in early 2006. It is an airborne L-band 2D Interferometric imaging system with dual polarizations. Its U-shape array consists of 36 elements and 575 baselines. The minimum element spacing Δu is 0.7λ. The angular resolution is between 5° and 7°. HUT-2D is recognized as one of the demonstrators of the SMOS (Soil Moisture and Ocean Salinity) mission for the ESA (European Space Agency) to validate the feasibility of retrieving soil moisture and ocean salinity using 2D interferometric radiometers. Successful ground and air based tests were conducted to study the interferometric theory and instrument calibration. The first test flight was carried out on May 29, 2006 (Kainulainen et al, 2007).

Soil Moisture and Ocean Salinity (SMOS) is the first space mission for an interferometric imaging radiometer. The Microwave Imaging Radiometer using Aperture Synthesis (MIRAS) was proposed to the European Space Agency (ESA) in 1994 and approved in 1998 as the only payload onboard the SMOS mission (Martin-Neira et al, 1994; Kerr et al, 2000). MIRAS adopts a Y-shape 2D array and consists of a central structure and three deployable arms, each of which has three segments, see Fig.9.

Fig. 9. Y-shaped antenna array of MIRAS and SMOS spacecraft of ESA

During launch, these arms are folded-up, but soon after separation from the launch vehicle they are gently deployed via a system of spring-operated motors and speed regulators. There are 69 antenna elements – the so-called LICEF receivers, which are equally distributed over the three arms and the central structure at a minimum distance of 0.875λ. The length of each arm is about 4 meters. The scheduled launch date of SMOS was postponed until November 2009. From an altitude of 755 km in Sun synchronous orbit, the element antenna will view an area of almost 3000 km in diameter. However, due to the interferometric principle and the Y-shaped antenna array, the field of view is limited to a hexagonal shape about 1000 km across called the 'alias-free zone'. This area corresponds to observations where there is no ambiguity in the phase-difference. The ground resolution is better than 50km for soil moisture and is better than 200km for ocean salinity.

Geostationary Synthetic Thinned Aperture Radiometer (GeoSTAR) is another Y-shaped snapshot interferometric imaging radiometer supported by NASA's IIP program and developed by the Jet Propulsion Laboratory (JPL) (Lambridtsen et al, 2004, 2006). This microwave atmospheric sounder will be onboard the geostationary GOES weather satellites operated by NOAA and will be in orbit by 2014. GeoSTAR will use the same channels as AMSU-A/B at 50GHz and 183GHz for oxygen and water vapour sounding. In total, 768 elements at 183GHz will be equally placed in a Y-shape structure. A more complicated array is selected for the 50GHz channel, 3 F-shaped arms with two kinds of aperture sizes are employed to avoid the structure interference with 183GHz and to improve the effective aperture ratio. Distance between adjacent elements is 3.5λ , which results in a field of view (FOV) of 17.5° from the geostationary orbit. In order to measure global temperature and humidity distribution, GeoSTAR is intending to provide continuous observations with a

spatial resolution of 25~30km. It is expected to be the first microwave sounder in geostationary orbit for atmospheric measurement. A Y-shape demonstrator with 24 elements has been completed and a series of experiments are being conducted. The demonstrator has 4 channels within 50~55GHz (Tanner et al, 2006).

4.3 2-D time-shared scanning imaging system

The 2-D snapshot imaging systems with high time resolution is very suitable for the real-time imaging observations, particularly for the case of observing from a fast moving platform at low earth orbit. However, for non-real-time observations, for example, when the platform is relatively stationary compared to observational targets and the targets' natural radiation is slowly changing, it would be too expensive to apply the traditional 2-D snap short imaging systems. Furthermore, for space borne applications, the overall cost with many element and channels, the resources required in power supply and mass of the 2-D snap shot systems are all difficult obstacles to overcome.

Recently, the time-shared scanning scheme with low hardware complexity has attracted more and more attention. It has potential to overcome the problems caused by the bulky and complex hardware of snapshot systems. Time-shared scanning scheme basically refer to applying a few antenna elements to compose a simple array, and integrally moving the array or separately moving the elements to get more spatial frequency samples. After a scanning cycle period, a full u-v sampling coverage can be achieved, and the brightness temperature image can be reconstructed by inversing these saved u-v measurement data. Time shared imaging schemes can greatly reduce the number of antenna elements and receivers. Thus the system cost could be cut down and the imaging spatial resolution could also be further increased since the overall complexity of the system has been dramatically reduced.

Depending on the means of movement of the thinned array, the time shared scanning scheme can be divided into sliding scan and rotating scan. Sliding scan means the antenna elements slide along some guide rails back and forth during the sample measurement process. The guide rails of every antenna elements are usually straight lines. For example, in the T-shaped and Y-shaped sliding scans, see Fig. 10, each antenna element is sliding along its respective guide rail at a different pace. After carefully designing the movement strategy of each element, all the baselines that needed to cover the full u-v plane will be aligned during a scanning cycle period, which have the same sampling effect as a uniformly distributed array along the rails.

The sliding scan has some disadvantages. It requires a complicated mechanical control system. The heavy mechanical attrition in the sliding process will greatly shorten the lifetime of the system. More importantly, it is hard to keep the system's momentum balanced. All these disadvantages limit its space borne application. Therefore, it is only fit for the ground-based imaging systems.

The other time-shared sampling scan, the rotation scan, is implemented by rotating all the coplanar antenna elements around a fixed axis to obtain more observation baseline vectors and more u-v sampling points. It has obvious advantages when compared to sliding scan in that it adopts the simpler and more reliable rotation control components, generates less

kinetic friction with high system stability, and is easier to achieve rotational balance. It is then more appropriate for space borne applications.

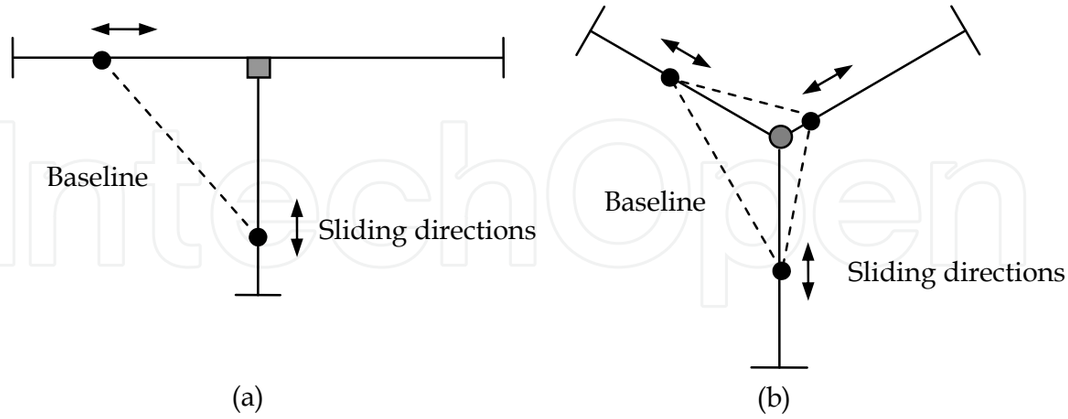

Fig. 10. Schematic diagrams of T-shaped sliding scan (a) and Y-shaped sliding scan (b)

There are generally two kinds of rotation scans, the synchronous rotation scan and the asynchronous rotation scan. The former one means the antenna array is integrally rotating around a fixed axis, and all the elements have the same angular rotation speed (Wu et al, 2005b), see Fig. 11. The latter one means the antenna elements are separately rotating around a same axis with different angular rotation speeds. In this type of rotational scan, the antenna elements are divided into two groups. The elements in one group have the same angular rotation speed and arm length, but different speeds to the elements in another group. This configuration is somewhat like a clock, especially when each group has only one antenna element, so it is also called a clock scan (Wu et al, 2007), see Fig. 12.

The sampling grid of synchronous rotation scan is composed by concentric circles, as shown in Fig. 11 (b). Each sampling circle corresponds to a physical baseline. An N elements array can form $N(N-1)/2$ physical baselines and scan out $N(N-1)/2$ sampling circles. The more uniform the concentric circles are, the better the image reconstruction is. Therefore, in order to get a rather uniform grid and reduce the system complexity at the same time, the antenna array with nonredundant linear distributed baselines is preferred. For linear arrays, there does not exist such an alignment with zero redundant baselines for N>4. For planar arrays, the array optimization is needed, and must resort to nonlinear iterative methods. Some good results of arbitrary planar array and circular array have been achieved by using simulated annealing method (Sun et al, 2005). Same as the traditional 2-D snapshot imaging system, the total number of antenna elements of the synchronous rotation scanning system is also determined by the required spatial resolution. Because its longest baseline, being about $N(N-1)/2 \cdot \Delta u$, is related to the number of antenna elements N, the system complexity of synchronous rotation scan can be reduced to about the square root of the 2-D snapshot system complexity, which is in the order of N^2.

The scanning tracks of the sampling point on the u-v plane of the clock scan scheme are some kind of spiralling curves, as shown in Fig. 12(b). The uniformity and the average gaps between the spirals are primarily determined by the speed ratio between the two antenna groups. As the speec ratio approaches 1, the more uniform the sampling grid and the longer

the scanning cycle period would be. The largest and shortest baselines of a clock scan are respectively determined by the sum and difference of the lengths of the long arm and short arm. Any length of baselines between the shortest and largest baselines can

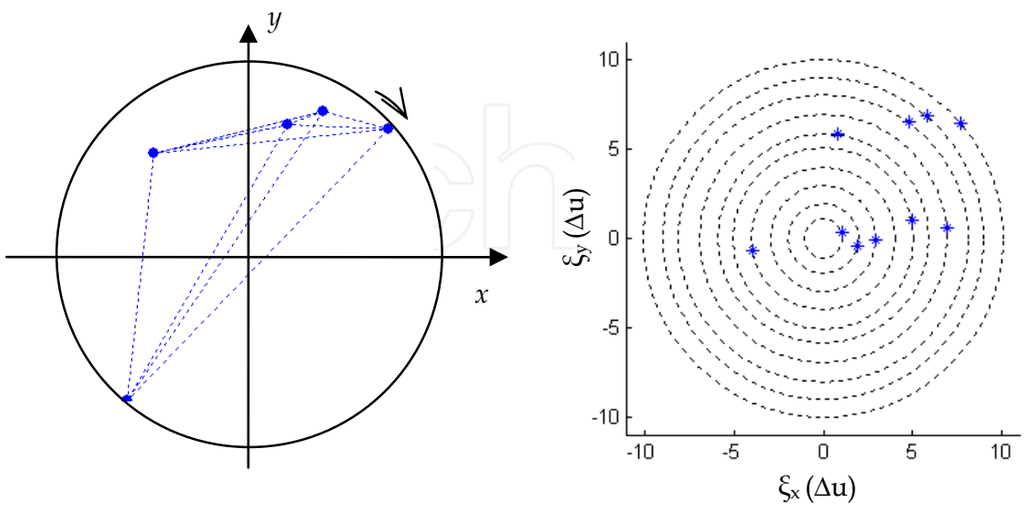

Fig. 11. Schematic diagrams of synchronous rotation scan scheme with 5-elements (a) and its sampling scanning trajectory (b)

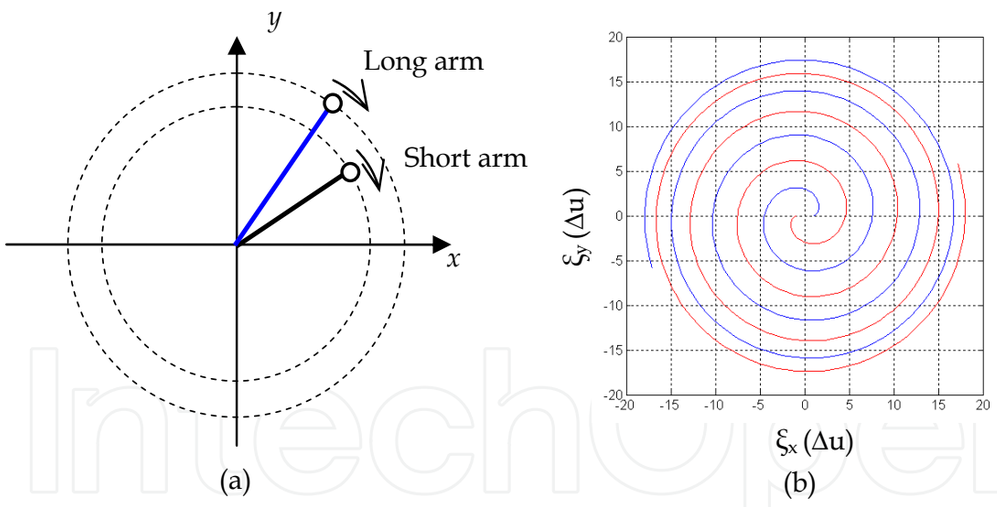

Fig. 12. Schematic diagrams of clock scan scheme with two elements (a) and its sampling scanning trajectory (b)

be created by the two antenna groups during their inconsistently rotating scan. Therefore, in some particular cases, the system complexity can be optimally reduced to the simplest limit of only two antenna elements and receivers. With the simplest two antenna elements configuration, the clock scan can still conveniently and efficiently achieve a full u-v sampling coverage. This is the most outstanding advantage of the clock scan. However, the scanning cycle period can be very long.

The number of arms of a clock scan system is determined by the image refresh time limit and system required brightness measurement sensitivity. Thus in order to increase the system time resolution and measurement sensitivity, the multi-arm configuration can be adopted, such as 2–2 arms, 4-4 arms and so on. A 4-4 arms system is shown in Fig. 13. The symmetric distributed multi-arm configurations are also helpful to keep the balance of the rotating system. According to the basic concepts of the clock scan, it can be extended to various specific transformations, such as step rotation scan, variable speed continuous rotation scan and swing rotation scan, etc.

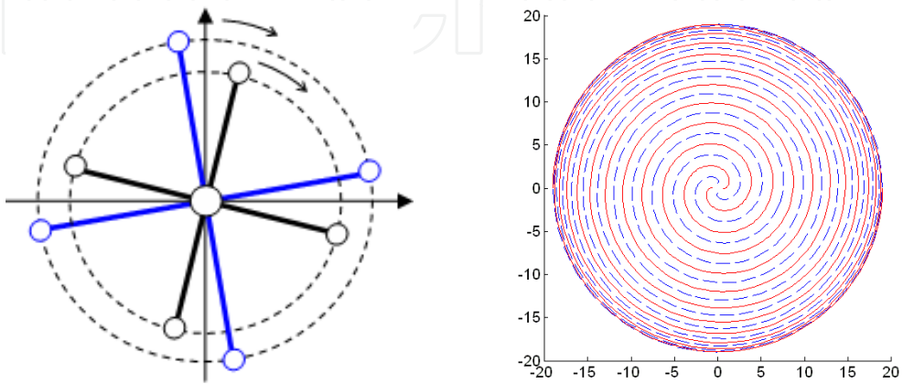

(a) (b)

Fig. 13. 4-4 arms clock scan system (a) and its sampling tracks on the u-v plane (b)

5. Brightness temperature retrieval methods

The visibilities or the samplings in the spatial frequency domain, measured by complex cross correlating between the signals received by two element antennas, are the primary measurements of synthetic aperture interferometric radiometers. They are related to the observed scene or target brightness temperature by a Fourier type transform. Accurate and fast inversion of the visibility data into the brightness temperature image is a critical step of the interferometric imaging technology. Due to different sampling schemes, there are still problems needing to be further explored.

In the ideal case, the visibilities and the brightness temperature are correlated by Fourier transform. However, in practice, the imperfections of the sampling process and various errors in receiving channels will influence the visibility measurement and damage the Fourier relationship. These system imperfections are mainly the channel imbalance and mutual coupling, antenna pattern distortion and mismatches, band width fringe washing effects and so on. All the distortions and amplitude/phase errors must be characterized and calibrated even though it is hard work. These calibration techniques include the distributed in-phase/out-phase noise injection technique applied in MIRAS system (Lemmetyinen et al, 2007) and I/Q vectors modulator technique applied in CAS-C/X system (Wu et al, 2004 and Liu et al, 2005b). After all the receiver channel errors have been corrected, the image reconstruction algorithms can be applied to the revised visibility data. In the following sub-sections, a few general brightness temperature retrieval approaches are introduced.

5.1 G-matrix inversion method

The G-matrix inversion method is a combination of system calibration and imaging reconstruction. It is very effective and convenient for small array systems, especially for 1-D imaging systems. It has been applied in the ESTAR system (Ruf et al, 1988 and Le Vine et al, 1994). The G-matrix inversion is based on numerical computation. Since the integral relation between the visibilities and brightness temperatures can be made discrete to a summation equation when considering that the brightness temperature distribution is represented by a sequence of discrete point sources. Then associate with the sampling theorem, the integral can be replaced by a vector product, and the set of visibility samples can be combined in matrix form,

$$V_{2N+1} = G_{(2N+1)\times M} \cdot T_M \tag{3}$$

where V_{2N+1} is the column vector of $2N+1$ visibility components including the zero-baseline and the real and imaginary part of other N baselines visibilities; T_M is the column vector of M discrete brightness temperature; G is the system modulation matrix including system errors. Each element of the G matrix corresponds to a measured spatial impulse response of each baseline correlation. The G matrix can also be recovered by deconvolving the measurements of known models of a brightness temperature scene. All the system imperfections and errors as well as the Fourier relations are embedded in the G matrix. Other calibration and revision works are not necessary any longer after the G matrix was measured.

The image reconstruction is a matter of inversing Equation (3). Generally the G matrix is not square, and the M brightness temperatures are as many as more than 3 times of the measured $2N+1$ visibility components. For this unconditioned problem, the inversion has to be computed by using a minimization algorithm in the least square sense. A direct way is to use the Moore-Penrose pseudo inverse method, which is expressed as

$$T = G^H (G \cdot G^H)^{-1} \cdot V \tag{4}$$

where H denotes the conjugate transpose. It is difficult to apply the G matrix method to a large 2-D array system, because the complexities of physically measuring the impulse response and mathematically inversing the G matrix are both increased with the square of the number of array elements. In addition, the drifts of receiver parameters require a periodic calibration. It is impractical to periodically refresh the large G matrix for space-borne applications.

5.2 Fourier Transform inversion method

When the receiver amplitude/phase errors can be calibrated and the system imperfection is small, the Fourier based inversion algorithms can be applied. The standard rectangular FFT can be directly applied to the rectangular sampling grid arrays, such as the U-shaped, T-shaped and X-shaped arrays. From signal theory it is known that the hexagonal sampling grid requires the minimum density of u-v samples to recover the image with a specified aliasing level. It has 13.4% less samples than rectangular sampling grid. Thus in order to process the visibilities sampled on hexagonal grids given by Y-shaped or triangular-shaped

arrays, the hexagonal FFT algorithm has been developed (Camps et al, 1995 and 1997). Hexagonal FFT can use the standard rectangular FFT routines to quickly implement a reversible transform between the hexagonal grid in spatial domain and another hexagonal grid in spatial frequency domain without interpolation processes. It is noted that, the Y-shaped array is better than the triangular-shaped array because when having the same hardware complexity it has a larger sampling coverage and associated better spatial resolution. Therefore, as the optimal 2-D snapshot array configuration, the Y-shaped array was adopted by the MIRAS/SMOS system.

On the other hand, for the polar girds and spiral grids sampled by rotation scanning system, it seems no such fast direct algorithms exist to do Fourier transformations on such non rectangular grids. What one can do is to apply interpolation method to convert these irregular girds to a uniform grid that is proper for FFT routines and then use FFT to do the reconstruction. Such kind of methods are called interpolation based Fourier methods. There are mainly two interpolation based Fourier methods that have been proposed so far, the rectangular grid based Gridding method (Beatty et al, 2005) and the pseudo-polar grid based 1-D interpolation pseudo-polar FFT method (Zhang et al, 2007).

The Gridding method is a convolution based resampling technique which is widely used to convert the random non-uniform data to a rectangular grid. The procedure is that, firstly estimating the sampling density of the non-uniform data and compensating the data by dividing their density; then convolving the compensated data with a specific kernel function to recover the corresponding initial function and resample it on the required Cartesian grid, finally performing the standard IFFT to reconstruct the brightness temperature image. The density estimation and convolution kernel are the most important factors that are responsible for the reconstruction accuracy. Generally the Voronoi diagram method can be used to calculate the sampling density and the widely accepted Kaiser-Bessel kernel function can be used to do the convolution.

The interpolation pseudo-polar FFT method is specifically proposed for the polar grid of concentric circles sampled by synchronous rotation scanning system. Using two steps of 1-D interpolations, the angular interpolation and radial interpolation, the polar grid can be converted to a pseudo-polar grid, which is composed by concentric rectangles and equi-sloped rays, as shown in Fig. 14. Then applying 1-D FFT and fast FRFT (Fractional Fourier Transform), the spatial frequency data in pseudo-polar grid can be transformed to a Cartesian grid in the spatial domain. The interpolation pseudo-polar FFT method has a promising imaging performance by virtue of high accuracy of 1-D interpolations and fast computational operations.

5.3 Non linear iterative optimization method

For the systems without accurate calibration or missing some baselines, especially when large antenna pattern errors and large sampling non-uniformity exist, the inversion of the visibility equation dose not have an analytical solution. In this case, iterative optimization techniques, such as the Clean method and maximum entropy method (MEM), can be used to deal with this kind of problems.

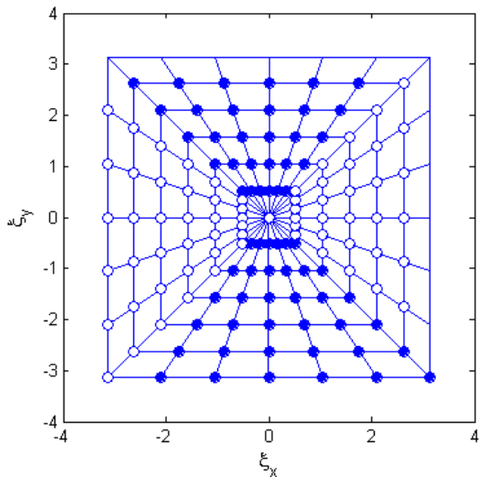

Fig. 14. Schematic diagram of pseudo-polar grid

The Clean method is the most popular method used in radio astronomy with interferometric imaging systems. Because of incomplete sampling in the u-v plane and atmosphere path distortion, the directly reconstructed image has large amount of noise. Consequently, the direct reconstruction is called dirty image and the equivalent array factor AF is called a dirty beam. The Clean method is to extract the useful information and remove the noise to obtain a high quality image. It first assumes the radio source is represented by a number of point sources, the stars, in an empty FOV, then it finds the position and strength of the most brilliant peak in the dirty image and subtracts the dirty beam centered at this point with a damping factor from the dirty image. This process is repeated until the residual image is no longer significantly above the noise-level. Finally the clean image is obtained by convolving the accumulated point sources model with an idealized clean beam, usually a Gaussian beam with the same half-power beam width as the dirty beam. From the principles it is clear that, the Clean method would have difficulties to directly applied for earth observation case because the earth targets appears as an extended thermal source filling the FOV and not a set of point sources. Although extensions of the Clean method for extended targets imaging are studied (Camps et al, 1998), regardless whether it is effective, it still requires much prior knowledge of the targets in the FOV.

The maximum entropy method (MEM) is another effective method applied to optimizing the synthetic aperture images in radio astronomy (Skilling & Bryan, 1984). It originated from maximum probability distribution in statistical physics, and particularly useful in solving the ill-posed problem with incomplete measurement data. The MEM tries to define a concept of entropy to characterize the solutions as well as prior knowledge and then obtains a solution which has the maximum entropy among all the solutions in a certain noise level. In order to successfully find the best solution being closest to the real one, enough constrains must be imposed to the infinite solution space, such as the positive constraint (all the elements are positive), the smoothness constraint (minimum variance of its second derivative) or other prior knowledge.

The Clean method and MEM method are both nonlinear, and consequently not easy to treat mathematically. It requires time consuming iterative procedures and large storage space.

Moreover, the prior knowledge of the observation scene is necessary even for extended targets. The practical applications of these nonlinear iterative methods for earth observations are not yet mature.

6. Application prospects

The interferometric passive microwave imaging system has a wide area of applications, including all the traditional microwave radiometer application areas and some other specific areas, such as high spatial resolution earth observation in geostationary Earth orbit or low frequency band, security detection of hidden weapons or other contrabands on the ground.

Geostationary earth orbit (GEO) microwave observation is an attractive potential application for interferometric imaging techniques. In order to implement accurate and timely monitoring of disastrous weathers such as typhoons, rainstorms or other severe convective weather events and increase weather forecasting precision, some prestigious government space agencies such as NASA and ESA are devoted in developing GEO meteorological satellite with microwave imaging system. China is also planning to launch a microwave imaging sounder on a GEO weather satellite. The main challenge of GEO applications is to realize a high spatial resolution at such a high orbit. One will meet great difficulty if they simply adopt the traditional real aperture microwave radiometer because the physical size of antenna will be too large even in millimeter band, not to mention how to scan it in order to get an image. Applying interferometric imaging technique is a promising way to overcome this problem. Especially if the scene becomes a slow moving/variable target, the time shared scan scheme, such as rotation scanning scheme, can be applied. This will further reduce the complexity of the system. Now the foresight study for rotation scanning interferometric millimeter atmospheric temperature imaging sounders for GEO satellite application have been carried out by NASA, ESA and also in China. The breakthroughs of this technology will help human beings understand the global weather system better and also giving more precise weather forecasts in the future.

Another important potential application of the interferometric imaging technique is the solar wind observation in solar polar orbit. The solar wind plays an essential role in shaping and stimulating planetary magnetospheres and ionic comet tails. It is a prime source of space weather. Coronal Mass Ejections (CMEs) produce the largest transient disturbances in the solar wind, which are closely related to solar activity, interplanetary shocks and geospace environment changes. With the development of Aerospace technology, precise forecasts of large disturbance events are being put on the agenda. Several solar-terrestrial space exploration projects are proposed in China, for example, the Solar Polar Orbit Radio Telescope (SPORT) project proposed by CSSAR/CAS (Center for Space Science and Applied Research, Chinese Academy of Sciences) (Wu et al, 2005c, 2006). In the SPORT mission, it is planned to launch a space-based observatory into solar polar orbit, and implement the first ever remote sensing measurements of the solar wind from the polar region above the sun outside of the ecliptic plane. The main objectives of SPORT are tracing the propagation of high density plasma clouds within about 1 square AU area near the ecliptic plane, imaging its intensity distribution and forecasting the propagation and intensity trend. Therefore, it is very helpful for geospace weather and environment forecast, and also for solar physics and

plasma physics studies. The sensitive frequency of plasma clouds is very low. If using conventional real aperture radiometry technique, the required physical aperture of the antenna would be far exceed the mechanical production ability and rocket load capacity. Therefore, the interferometric imaging technique with rotational scanning scheme is adopted in SPORT project. It will apply the clock scan scheme with two sets of rotating arms. Each set of arms is composed of four long booms extended for 70-80 meters and 90 degree apart. The spacecraft is located in the rotational centre and will rotate together with one set of the arms. It is therefore a spin stabilized spacecraft. The rotation axis is pointing to the Sun all the time. More details can be read in (Wu et al, 2005c, 2006).

7. Conclusions

Interferometric imaging radiometer technology was introduced into the area of Earth observation from radio astronomy technology more than 20 years ago. Due to the differences between astronomy observation and that of the earth observation, the technology has gone through redevelopment over the past 20 years.

During redevelopment, there have been two main technical trends. The first one is to be more and more complicated by increasing the number of elements to reach higher spatial resolutions and at the same time to keep its radiometric sensitivity, such as the snapshot 2-D Y-shape designs. This technical trend has relied on the fast development of IC technology that enables us to integrate thousands of correlators into one chip. A representative of this technical approach is the MIRAS payload on SMOS mission by ESA. The other technical trend is trying to reduce the number of elements and using time shared scan scheme in order to cover the complete u-v plane. The initial driving force behind this trend is the necessity to keep the system design simple and manageable. Along this line, as described in this chapter, we have discovered the secrets inside the technology, i.e. the very basic configuration of the interferometric imaging system. It, in fact, can be represented by only two element antennas using the clock scan scheme. Any spatial resolution and radiometric sensitivity can be reached by using this two-element clock scan as basic building blocks in principle.

In November 2009, the first ever space mission SMOS using this new technology for earth observation will be launched. We expect a successful demonstration of this technology by SMOS mission. After this, in the near future, we expect to see more missions using this technology such as the geo-sounder on board of either a US weather satellite or a Chinese weather satellite since both are working on it. We would also expect the SPORT mission to be launched before 2020 using 4-4 element clock scan to take images of the interplanetary CMEs and also the universe background emission at 15MHz. It is certainly an exciting technology but perhaps not the dominating technology in the area of passive microwave remote sensing due to its complexity compared to tradition real aperture radiometers. Therefore, the traditional microwave radiometer will still exist. The users will select from both in order to keep the best performance over cost and technical feasibility.

8. References

Anterrieu, E., Waldteufel, P. & Lannes, A. (2002). Apodization functions for 2-D hexagonally sampled synthetic aperture imaging radiometers, *IEEE Transactions on Geoscience and Remote Sensing*, Vol.40, No.12, pp.2531-2542, ISSN: 0196-2892

Beatty, P.J., Nishimura, D.G. & Pauly, J.M. (2005). Rapid gridding reconstruction with a minimal oversampling ratio, *IEEE Transaction on Medical Imaging*, Vol.24, No.6, pp.799- 808, ISSN: 0278-0062

Camps, A., Bara, J., Corbella, I. & Torres, F. (1995). Visibility inversion algorithms over hexagonal sampling grids, *Proceedings of Soil Moisture and Ocean Salinity Measurements and Radiometer Techniques*, *ESA-ESTEC workshop*, pp.109–114, Noordwijk, The Netherlands, Apr. 1995, ESA document WPP87

Camps, A., Bara, J., Corbella, I. & Torres, F. (1997). The Processing of hexagonally sampled signals with standard rectangular techniques: application to aperture synthesis interferometer radiometer, *IEEE Transaction on Geoscience and Remote Sensing*, Vol.35, No.1, pp.183-190, ISSN: 0196-2892

Camps, A., Bara, J., Torres, F. & Corbella, I. (1998). Extension of the Clean technique to the microwave imaging of continuous thermal sources by means of aperture synthesis radiometers, *Journal of electromagnetic waves and applications*, Vol.12, No.3, pp.311-313, ISSN: 0920-5071

Corbella, I., Duffo, N., Vall-llossera, M., & Camps, A. (2004). The visibility function in interferometric aperture synthesis radiometry, *IEEE Transaction on Geoscience and Remote Sensing*, Vol.42, No.8, pp.1677-1682, ISSN: 0278-0062

Dong, X.L., Wu, J., Zhu, S.Y. et al. (2000). The design and implementation of CAS C-band interferometric synthetic aperture radiometer, *Proceedings of IGARSS'00*, Vol.2, pp.866-868, ISBN: 0-7803-8743-0, Honolulu, Hawaii, USA, July 2000, IEEE, New York

Guha, A., Jacobs, J.M., Jackson, T.J. et al. (2003). Soil moisture mapping using ESTAR under dry conditions from the southern great plains experiment (SGP99), *IEEE Transactions on Geoscience and Remote Sensing*, Vol.41, No.10, pp.2392-2397, ISSN: 0196-2892

Harris, F. J. (1978). On the use of windows for harmonic analysis with the discrete Fourier transform, *Proceedings of IEEE*, Vol.66, Issue.1, pp.51-83, ISSN: 0018-9219

Ishiguro, M. (1980). Minimum redundancy linear arrays for a large number of antennas, *Radio Science*, Vol.15, pp.1163-1170, ISSN: 0048-6604

Kainulainen, J., Rautiainen, K., Tauriainen, S., Auer, T., Kettunen, J. & Hallikainen, M. (2007). First 2-D interferometric radiometer imaging of the earth from an aircraft, *IEEE Geoscience and Remote Sensing Letters*, Vol. 4, No. 2, pp. 241-245, ISSN: 1545598X

Kerr, Y., Font, J., Waldteufel, P., Camps, A., Bara, J., Corbella, I., Torres, F., Duffo, N., Vallilossera, M. & Caudal, G. (2000). New radiometers: SMOS-a dual pol L-band 2D aperture synthesis radiometer, *IEEE Aerospace Conference Proceedings*, Vol.5, pp.119-128, ISBN: 0-7803-5846-5, Big Sky, MT, USA, Mar. 2000, IEEE New York

Lambrigtsen, B., Wilson, W., Tanner, A., Gaier, T., Ruf, C. & Piepmeier, J. (2004). GeoSTAR - a microwave sounder for geostationary satellites, *Proceedings IGARSS '04*, Vol. 2, pp. 777-780, ISBN: 0-7803-8742-2, Anchorage, AlasKa, USA, Sept. 2004, IEEE New York

Lambrigtsen, B. (2006). GeoSTAR: Developing a new payload for GOES satellites, *Proceedings of the 2006 IEEE/AIAA Aerospace Conference*, pp.1-9, ISBN: 0-7803-9545-X, Big Sky, Montana, Mar. 2006

Le Vine, D.M., Griffis, A.J., Swift, C.T. et al. (1994). ESTAR: a synthetic aperture microwave radiometer for remote sensing applications, *Proceedings of the IEEE*, Vol.82, No.12, pp.1787-1801, ISSN: 0018-9219

Le Vine, D.M. (1999). Synthetic aperture radiometer systems, *IEEE Transaction on Microwave Theory and Techniques*, Vol.47, No.12, pp.2228-2236, ISSN: 0018-9480

Le Vine, D.M., Koblinsky, C., Howden, S., et al. (2000a). Salinity measurements during the gulf stream experiment, *Proceedings of IGARSS'00*, Vol.6, pp.2537-2539, ISBN: 0-7803-6359-0, Honolulu, HI, USA, Jul. 2000, IEEE New York

Le Vine, D.M. et al. (2000b). Development of a two dimensional synthetic aperture radiometer at L-band, *Proceedings of IGARSS'00*, pp.994-2996, ISBN: 0-7803-6359-0, Honolulu, HI, USA, Jul. 2000, IEEE New York

Le Vine, D.M., Jackson, T.J., Swift, C.T. et al. (2001). ESTAR Measurements during the southern great plains experiment (SGP99), *IEEE Transaction on Geoscience and Remote Sensing*, Vol.39, No.8, pp.1680-1685, ISSN: 0196-2892

Le Vine, D.M., Haken, M. & Swift, C.T. (2004). Development of the synthetic aperture radiometer ESTAR and the next generation, *Proceedings of IGARSS'04*, Vol.2, pp.1260-1263, ISBN: 0-7803-8742-2, Anchorage, AlasKa, USA, Sept. 2004, IEEE New York

Le Vine, D. M., Jackson, T. J., Haken, M. (2007). Initial images of the synthetic aperture radiometer 2D-STAR, *IEEE Transaction on Geoscience and Remote Sensing,* Vol.45, No.11, pp.3623-3632, ISSN: 0196-2892

Lemmetyinen, J., Uusitalo, J., Kainulainen, J. et al. (2007). SMOS calibration subsystem, *IEEE Transactions on Geoscience and Remote Sensing*, Vol.45, No.11, pp.3691-3700, ISSN: 0196-2892

Liu, H., Wu, J. et al. (2004). The CAS airborne X-band synthetic aperture radiometer: system configuration and experimental Results, *Proceedings of IGARSS'04*, Vol.3, pp.2230-2233, ISBN: 0-7803-8742-2, Anchorage, AlasKa, USA, Sept. 2004, IEEE New York

Liu, H., Wu, J., Wu, Q. (2005). Analysis and calibration of the channels error of synthetic aperture radiometer, *ACTA Electronica Sinica*, Vol.33, No.3, pp.402-406, ISSN: 0372-2112

Martin-Neira, M., Menard, Y., Goutoule, J.M. & Kraft, U. (1994). MIRAS: A two-dimensional aperture synthesis radiometer, *Proceeding of IGARSS'94,* Vol.3, pp.1323–1325, ISBN: 0-7803-1497-2, Pasadena, CA, USA, Aug 1994, IEEE New York

Rautiainen, K., Valmu, H., Jukkala, P. et al. (1999). Four two-element prototype of the HUT interferometric radiometer, *Proceedings of IGARSS'99*, Vol.1, pp.234-236, ISBN: 0-7803-5207-6, Hamburg, Germany, Jun. 1999, IEEE New York

Rautiainen, K., Butora, R., Auer, T. et al. (2003). Development of airborne aperture synthetic radiometer (HUT-2D), *Proceedings of IGARSS'03*, Vol.2, pp.1232-1234, ISBN: 0-7803-7929-2, Toulouse, France, July 2003, IEEE New York

Ribo, S. (2003). Research on image validation and signal processing of aperture synthesis radiometry, *Internal ESTEC Working Paper*, No.2182, pp.81-92, European Space Research and Technology Centre, European Space Agency (ESTEC-ESA)

Ruf, C.S., Swift, C.T., Tanner, A.B. & Le Vine, D.M. (1988). Interferometric synthetic aperture microwave radiometry for the remote sensing of the earth, *IEEE Transaction on Geoscience and Remote Sensing*, Vol. 26, No.9, pp. 597–611, ISSN: 0196-2892

Ruf, C.S. (1993). Numerical annealing of low-redundancy linear arrays, *IEEE Transactions on Antennas and Propagation*, Vol.41, No.1, pp.85-90, ISSN: 0018-926X

Ruf, C., Principe, C. et al. (2002). Lightweight fainfall fadiometer STAR aircraft sensor, *Proceedings of IGARSS'02*, Vol.2, pp.850-852, ISBN: 0-7803-7536-X, Toronto, Canada, June 2002, IEEE New York

Ruf, C. & Principe, C. (2003). X-band Lightweight Rainfall Radiometer First light, *Proceedings of IGARSS'03*, Vol.3, pp.1701-1703, ISBN: 0-7803-7929-2, Toulouse, France, July 2003, IEEE, New York

Skilling, J. & Bryan, R.K. (1984). Maximum entropy image reconstruction: general algorithm, *Mon. Not. Roy. Astr. Soc.*, Vol.211, No.1, pp.111-124, ISSN: 0035-8711

Sun, W.Y., He, B.Y. & Wu, J. (2005). Optimization of fourier plane coverage of antenna arrays for SPORT, *PIERS Online*, Vol.1, No.5, pp.533-537, ISSN: 1931-7360

Tanner, A., Wilson, W., Lambrigsten, B., Dinardo, S., Brown, S., Kangaslahti, P., Gaier, T., Ruf, C., Gross, S., Lim, B., Musko, S. & Rogacki, S. (2006). Initial results of the Geosynchronous Synthetic Thinned Array Radiometer (GeoSTAR), *Proceedings of IGARSS'06*, pp.3968-3971, ISBN: 0-7803-9510-7, Denver, Colorado,USA, July 26, IEEE New York

Thompson A.R. & Schilizzi, R. T. (1986). *Interferometry and Synthesis Radio Astronomy*, John Wiley & Sons, ISBN-10: 0471806145, ISBN-13: 978-0471806141 , NewYork

Wu, J., Liu, H. et al. (2005a). Research Activity on Synthetic Aperture radiometry in CSSAR/CAS, *PIERS Online*, Vol.1, No.5, pp.538-542, ISSN: 1931-7360

Wu, J., Liu, H., Sun, W.Y. & Jiang, J.S. (2005b). Technological development and application prospect of synthetic aperture radiometer, *Remote Sensing Technology and Application*, Vol.20, No.2, pp.24-29, ISSN: 1004-0323

Wu, J., Liu, H., Sun, W.Y., Wang, C. & Shi, S. (2005c). Application of Synthetic Aperture Radiometer Technology in Solar Wind Remote Sensing, *Proceedings of PIERS 2005*, pp.23-26, ISSN 1559-9450, Hangzhou, China, August, 2005, The Electromagnetics Academy

Wu, J., Wang, C., Wang S. et al. (2006). Solar polar orbit radio telescope for space weather forecast, *Proceedings of the ILWS Workshop*, India, pp.215, ISBN: 81-87099-40-2, Goa, India, Feb. 2006, Quest Publications for ILWS

Wu, J., Zhang, C., Liu, H. et al. (2007). Clock scan of imaging interferometric radiometer and its applications, *proceedings of IGARSS'07*, pp. 244-5246, ISBN: 978-1-4244-1211-2, Barcelona, Spain, July 2007, IEEE New York

Wu. Q., Liu, H., & Wu, J. (2004). Image simulator for one-dimensional synthetic aperture microwave radiometer, *Proceedings of IGARSS'04*, Vol.6, pp. 3973- 3976

Zhang, C., Wu, J. & Sun, W.Y. (2007). Applications of pseudo-polar FFT in synthetic aperture radiometer imaging, *PIERS Online*, Vol.3, No.1, pp.25-30, ISSN1931-7360

Geoscience and Remote Sensing New Achievements

Edited by Pasquale Imperatore and Daniele Riccio

ISBN 978-953-7619-97-8
Hard cover, 508 pages
Publisher InTech
Published online 01, February, 2010
Published in print edition February, 2010

Our planet is nowadays continuously monitored by powerful remote sensors operating in wide portions of the electromagnetic spectrum. Our capability of acquiring detailed information on the environment has been revolutionized by revealing its inner structure, morphology and dynamical changes. The way we now observe and study the evolution of the Earth's status has even radically influenced our perception and conception of the world we live in. The aim of this book is to bring together contributions from experts to present new research results and prospects of the future developments in the area of geosciences and remote sensing; emerging research directions are discussed. The volume consists of twenty-six chapters, encompassing both theoretical aspects and application-oriented studies. An unfolding perspective on various current trends in this extremely rich area is offered. The book chapters can be categorized along different perspectives, among others, use of active or passive sensors, employed technologies and configurations, considered scenario on the Earth, scientific research area involved in the studies.

How to reference

In order to correctly reference this scholarly work, feel free to copy and paste the following:

Ji Wu, Hao Liu, Jingye Yan, Cheng Zhang and Weiying Sun (2010). Interferometric Imaging Technology for Microwave Radiometers, Geoscience and Remote Sensing New Achievements, Pasquale Imperatore and Daniele Riccio (Ed.), ISBN: 978-953-7619-97-8, InTech, Available from: http://www.intechopen.com/books/geoscience-and-remote-sensing-new-achievements/interferometric-imaging-technology-for-microwave-radiometers

INTECH
open science | open minds

InTech Europe
University Campus STeP Ri
Slavka Krautzeka 83/A
51000 Rijeka, Croatia
Phone: +385 (51) 770 447
Fax: +385 (51) 686 166
www.intechopen.com

InTech China
Unit 405, Office Block, Hotel Equatorial Shanghai
No.65, Yan An Road (West), Shanghai, 200040, China
中国上海市延安西路65号上海国际贵都大饭店办公楼405单元
Phone: +86-21-62489820
Fax: +86-21-62489821

IntechOpen